

Black Cumin Seed Extract as Copper Corrosion Inhibitor in H₂SO₄ 1M: An Experimental and Theoretical Study

Putri Elsa^{1*}, Sapriani Hamdiani¹, Emmy Yuanita¹, Saprizal Hadisaputra^{2*}

¹Departement of Chemistry, Faculty of Mathematics and Natural Sciences, University of Mataram, Mataram, Indonesia.

²Chemistry Education Division, Faculty of Teacher Training and Science Education, University of Mataram, Mataram, Indonesia.

Received: August 5, 2024

Revised: September 26, 2024

Accepted: October 27, 2024

Published: October 31, 2024

Corresponding Author:

Saprizal Hadisaputra

rizal@unram.ac.id

DOI: [10.29303/jppipa.v10i10.8739](https://doi.org/10.29303/jppipa.v10i10.8739)

© 2024 The Authors. This open access article is distributed under a (CC-BY License)



Abstract: Experimental corrosion tests and theoretical calculation were conducted to investigate the corrosion inhibition mechanism of black cumin seed extract for copper in 1 M H₂SO₄ solution. Electrochemical testing using electrochemical impedance spectroscopy (EIS) and potentiodynamic polarization (PDP) method showed that BCS adsorbed to form a protective layer on the copper surface with high inhibition efficiency at 500 ppm concentration (73,35%). Increasing the BCS concentration up to 500 ppm causes the charge transfer resistance increase in the EIS measurement, while the corrosion current density measured by PDP decreases. The values of charge transfer resistance and corrosion current density at 500 ppm BCS are respectively 3687 Ω.cm² and 2.86 μA.cm⁻². The BCS is a mixed inhibitor (anodic and cathodic) that adsorbs physically on the copper surface and obeys the Langmuir isothermal adsorption model. Quantum chemical calculation and molecular dynamic simulation show that the studied BCS molecules adsorb strongly on the copper surface with parallel orientation mode. The methyl linoleate (MLIN) molecules from BCS produce the most stable adsorption energy of the other studied compound molecules as a result of molecular dynamic simulation.

Keywords: Black cumin seed extract, copper corrosion, electrochemical impedance spectroscopy, potentiodynamic polarization, Density Functional Theory (DFT), Monte Carlo simulation

Introduction

Copper and its alloys are some metals widely used in various industrial fields. The utilization of this metal cannot be separated from its superior physical and chemical properties, which are easy to shape, can conduct heat and electricity well, and is more resistant to corrosion. This metal can form a protective layer on its surface in the form of copper oxide so that the corrosion rate of the copper underneath can be slowed down (Orozco-Cruz et al., 2017). This passive layer is only formed under neutral conditions, and its porous structure, the presence of cracks and corrosive ions such as chloride and sulfate ions cause damage to the copper corrosion cannot be avoided (Xu et al., 2018).

Corrosion deposits formed on copper surface can reduce its efficiency in conducting heat and electricity, affect its mechanical properties, and can contaminate the

environment and industrial products (Vargas et al., 2017; Xu et al., 2023). Copper corrosion treatment is generally carried out by sacrificial anode, anti-corrosion coatings and corrosion inhibitors (Essa et al., 2021; Xu et al., 2018 and Mollaamin, 2023). Metal and alloys can be protected from corrosion using corrosion inhibitors, according to Bilgic (2018), which is more effective than other methods. The type of corrosion inhibition by inhibitors can be in the form of adsorption of inhibitor molecules on the metal surface, forming a protective film, or forming insoluble complexes on the metal surface.

Inorganic corrosion inhibitors, such as chromates, phosphates, nitrates, and silicates, are commonly used in acid pickling. The purpose of adding inhibitors to the cleaning process is to prevent further corrosion of the metal material. Inorganic inhibitors are dangerous because they are toxic, carcinogenic, and pollute the

How to Cite:

Elsa, P., Hamdiani, S., Yuanita, E., & Hadisaputra, S. (2024). Black Cumin Seed Extract as Copper Corrosion Inhibitor in H₂SO₄ 1M: An Experimental and Theoretical Study. *Jurnal Penelitian Pendidikan IPA*, 10(10), 7765-7774. <https://doi.org/10.29303/jppipa.v10i10.8739>

environment (Vaghefinazari et al., 2022; Al-Amiery et al., 2022). Organic corrosion inhibitors can be used as corrosion inhibitors because they have high inhibition efficiency, are cheaper, and save environmentally (Zomorodian & Behnood, 2023). The action mechanism of inhibitors occurs through heteroatom groups such as nitrogen (N), sulfur (S) and oxygen (O), as well as double bonds in their structure, which can be adsorbed to form a protective layer on the metal surface.

Plant extracts contain metabolites that contain many heteroatom groups in their structure. These heteroatom groups can come from phenolic compounds, alkaloids, terpenoids, fatty acids, and carbohydrates (Saleh et al., 2018). According to research by Swathi et al. (2017), fatty acids can be used as corrosion inhibitors. Based on (BustosRivera-Bahena et al., 2024) research, fatty acids in palmitic acid, oleic acid, and ethyl linoleate are effective in inhibiting copper alloy corrosion. Fatty acid in pumpkin seed extract in research of Radi et al. (2021) also showed an inhibition efficiency of 95%. Carboxylic groups and π bonds in unsaturated fatty acids play a role in the adsorption of inhibitors on metal surfaces.

Black cumin seeds (*Nigella sativa*) contain 34-39% oil, which is composed of fatty acids, tocopherols, phytosterols, polyphenols, essential oils and another bioactive compound (Mazaheri et al., 2019). Based on Nivetha and Prasanna's (2016) research, black cumin seed extract contains major compounds such as linoleic acid, palmitic acid, eicosanoid acid, and ethyl palmitate. According to Rehioui et al. (2021), an unsaturated fatty acid in black cumin seed extract is 79%, so it has the potential to be used as a corrosion inhibitor. Research by (Souli et al. (2017) and Jayakumar et al. (2024) results obtained high inhibition efficiency of black cumin seed extract against iron corrosion. Black cumin extract and natural honey can also inhibit corrosion in water cooling systems based on Emad & Al-Rasheedi's (2015) research.

Based on the explanation above, this research focuses on the extraction of black cumin seeds, which are then tested for effectiveness as electrochemical copper corrosion inhibitors. Quantitative analysis of the major compounds from black cumin seed extract was carried out using GCMS. The investigation of the major compound that plays the most role in black cumin seed extract was analyzed theoretically through a computational approach using the DFT method and Monte Carlo Simulation.

Method

Extraction of black cumin seed

Black cumin seeds (100 g) were washed with distilled water and dried at room temperature (5 days). The dried black cumin seeds were then ground and pulverized. The black cumin seed powder was then

extracted using the soxhletation method using ethanol as a solvent (500 mL, 6 jam). The extract obtained was then concentrated with a rotary evaporator (40 °C) and stored in a sealed container at low temperature until use. The extract was calculated for yield and analyzed using Gas Chromatography-Mass Spectroscopy (GC-MS).

Preparation of Metal Specimen and Solution

The metal specimen used in this study is copper Cu (1 cm × 9 cm × 0,03 mm) with a purity of 99,90%. Copper was sanded using SiC sandpaper size P800 and P1500 until the surface was smooth. All parts of the specimen immersed in the test solution batch were coated using epoxy resin, except for the part where corrosion will be measured (1 cm²). The specimen was then cleaned using distilled water, rinsed with ethanol, rewashed with distilled water, and dried at room temperature.

The test batch solution consists of 1 M H₂SO₄ solution without and with the addition of black cumin seed extract. H₂SO₄ 1 M solution was prepared from concentrated sulfuric acid (98%) and distilled water. The addition of black cumin seed extract to the H₂SO₄ 1 M solution was carried out precisely according to the concentration variation of 100, 200, 300, 400, and 500 ppm.

Electrochemical measurements

The electrochemical measurement in this study used a three-electrode system at room temperature with Auto lab Metrohm dropsens instrument and controlled with Dropview8400 software. The electrochemical cell consisted of copper as the working electrode, Ag/AgCl in 3 M KCl as the reference electrode and platinum as an auxiliary electrode. All three electrode cells were inserted into the test batch solution (100 mL). Each working electrode was immersed in the test batch solution for 30 minutes before measurements were taken to achieve a stable state (Mzioud et al., 2020).

Electrochemical impedance spectroscopy (EIS) measurement refers to Tan et al.'s research (2021), using a frequency range of 100 kHz – 10 mHz at E_{OCP} with an amplitude of 5 mV. The EIS data was then analyzed using ZsimDemo3.20 software. Potentiodynamic polarization curves were determined with the polarization potential range applied to the working electrode, E_{OCP} ± 250, with a scan rate of 1 mV/s.

Theoretical and Computational Detail

Quantum chemical calculations are performed to support the experimental data. According to Hadisaputra et al. (2022), molecular structure, electron distribution and electron transfer from the inhibitor to the metal can be determined through quantum chemical calculations. Geometry and single-point energy optimization of the inhibitor molecule were carried out using the Density Functional Theory (DFT) method of

the B3LYP basis set with the 6-31G(d) function. All quantum chemical calculations were performed using Gaussian 09 software.

The quantum chemical parameters determined from the optimized compound are the molecular energies of the highest occupied molecular orbital (E_{HOMO}) and lowest unoccupied molecular orbital (E_{LUMO}), energy gap ($\Delta E = E_{HOMO} - E_{LUMO}$). Other parameters such as ionization potential (IP), electron affinity (EA), electronegativity (χ), hardness (η), global softness (σ), and transfer electron (ΔN) can be calculated using the following equations.

$$I = -E_{HOMO} \tag{1}$$

$$A = -E_{LUMO} \tag{2}$$

$$\eta = \frac{E_{LUMO} - E_{HOMO}}{2} \tag{3}$$

$$\sigma = \frac{1}{\eta} \tag{4}$$

$$\chi = \frac{(I+A)}{2} \tag{5}$$

$$\Delta N = \frac{\phi_{Cu} - \chi_{inh}}{2(\eta_{Cu} + \eta_{inh})r_{ir}^2} \tag{6}$$

Where ϕ (work function of copper) = 4,98 eV and $\eta_{Cu} = 0$ by assuming that a metallic bulk $I = A$ (Diki et al., 2021).

Monte Carlo Simulation

Monte Carlo simulation was used to understand the adsorption dynamics of the best inhibitor molecules on the metal surface. The most stable adsorbed inhibitor molecules on the metal surface have low energy. This simulation was performed using an adsorption locator and Forcite code with Material Studio 7.0 software. Optimization of the geometry of the inhibitor molecules was carried out using the COMPASS Forcefield (Hadisaputra et al., 2020). The simulation was performed on the Cu (111) supercell surface (20x20) in a simulation box (15 Å x 15 Å x 20 Å). A vacuum slab with a thickness of 5.0 nm was built on the Cu (111) plane. Each inhibitor molecule was simulated on the Cu surface with 100 water molecules.

Result and Discussion

Chemical Composition of Black Cumin Seed Extract

The extract of black cumin seed (BCS) from Soxhlet extraction with methanol as solvent obtained is yellowish brown. The yield of the extract obtained is 45,6%, which is almost the same as that studied by Alrashidi et al. (2022). The result of quantitative analysis using GCMS on black cumin seed extract can be seen in Table 1. Five major compounds were identified with a total area of 71,5%. Asam linoleate (25,12%) is the largest compound, and there is methyl linoleate (22,70%), methyl palmitate (6,66%), and palmitic acid (5,14%)

which belong to the fatty acid group. Quinoline group compounds were also identified, namely 4-cyclopentene-1,3-dione (7,64%) and carvacrol (4,35%).

Table 1. GCMS Analysis of Chemical Composition of Black Cumin Seed Extracts.

Compounds	Retention Time	Area (%)	
		Result	Ref
Terpinene-4-ol	8.738	0.50	0.65*
4-cyclopentene-1,3-dione	9.161	7.64	0.95*
Carvacrol	9.408	1.51	3.65*
Methyl myristate	11.165	0.40	0.15**
Myristic acid	11.330	0.11	0.18**
Methyl palmitic	11.896	6.66	11.31**
Palmitic acid	12.043	5.14	29.42**
Methyl linoleate	12.496	22.70	1.03**
Linoleate acid	12.688	25.12	54.96***
Stearic acid	12.730	1.40	2.98***

*Kabir, et al., (2020), **Nivetha & Prasanna, (2016), ***Alrashidi, et al., (2022)

Electrochemical Impedance Spectroscopy (EIS)

The Nyquist curve measured after immersion of the test specimen for 30 minutes in the batch solution with different concentrations and without BCS at 25°C is shown in Figure 1. Based on the research of (Sait et al., 2022), the capacitive loop in the impedance diagram forms a semicircle at high frequency, and the presence of Warburg impedance is characterized by a straight line in each diagram with concentration and without BCS at low frequency. It indicates that the addition of BCS to the corrosion batch solution does not change the copper corrosion mechanism. The Warburg impedance formed at a lower frequency indicates that the corrosion process is controlled by the diffusion of dissolved oxygen in H₂SO₄ 1M to the metal surface as well as mass transfer and soluble copper ions into the solution (Fu et al., 2018; Tan et al., (2018)).

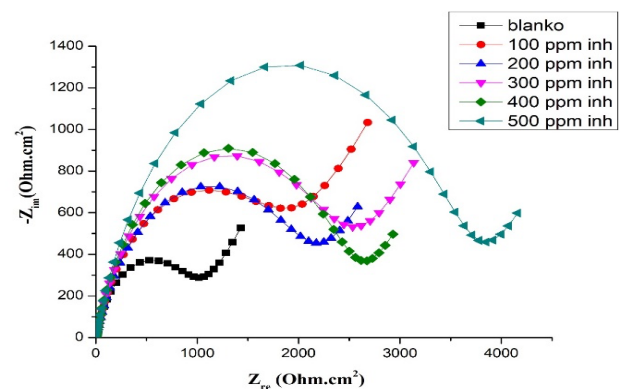


Figure 1. Nyquist diagram of copper in 1 M H₂SO₄ solution with concentration and without BCS at 25°C.

The capacitive loop formed at high frequency increases as the concentration of BCS increases, indicating that the value of R_{ct} increases. The inhibition efficiency of the inhibitor is determined from the charge transfer resistance value with the

addition of the inhibitor R_{ct} and $R_{ct,0}$ without the addition of the inhibitor. The charge transfer resistance value increased significantly from 982,5 $\Omega.cm^2$ in the batch solution without BCS to 3687 $\Omega.cm^2$ in the batch solution with 500 ppm CBS. It indicates that the adsorb BCS molecules form a dense protective layer on the copper surface. The highest copper corrosion inhibition efficiency was 73.35% at 500 ppm CBS.

$$EI\% = \frac{R_{ct} - R_{ct,0}}{R_{ct}} \times 100 \quad (7)$$

The capacitive value measured at high frequency indicates the charge transfer resistance (R_{ct}) and double-layer capacitance (C_{dl}). Adsorption of the inhibitor on the copper surface will change the double-layer capacitance value (Sedik et al., 2022). Referring to Table 2, the increase of CBS in the test medium causes the C_{dl} value to decrease. This indicates that CBS adsorbed on the copper surface, replacing water molecules.

The adsorption of the inhibitor on the metal surface causes the dielectric constant of the medium in the electric double layer to decrease and the thickness of the protective layer formed to increase. It causes the double-layer capacitance to decrease. The relationship of C_{dl} to the dielectric constant of the medium (ϵ), vacuum dielectric constant (ϵ_0), and the thickness of the protective layer (d) and the electrode surface area (A) is expressed by the following equation (Abdallah et al., 2022).

$$C_{dl} = \frac{\epsilon_0 \epsilon A}{d} \quad (8)$$

Table 2. Impedance Parameters of Copper in 1 M H₂ SO₄ with and without BCS Concentration Variation at 289K

C (ppm)	Rs ($\Omega.cm^2$)	C _{dl} (×10 ⁻⁵ S.S ⁿ)	R _{ct} ($\Omega.cm^2$)	W (m $\Omega.m^2$)	EI%
Blank	0.94	21.30	982.5	5.68	-
100	1.01	16.10	1871	2.96	47.48
200	1.02	12.20	2110	5.10	53.50
300	0.74	8.10	2440	3.65	59.73
400	1.52	6.91	2533	6.41	61.21
500	1.64	4.39	3687	5.39	73.35

Potentiodynamic Polarization (PDP)

The effect of BSC addition on copper corrosion test media can be seen from the Tafel polarization curve in Figure 2. Corrosion parameters such as current density and corrosion potential can be known from the intersection point of the two extrapolated lines of the anodic and cathodic curves. The electrochemical parameters that can be calculated are the corrosion potential (E_{corr}), corrosion current density (I_{corr}), anodic Tafel slope (β_a), cathodic Tafel slope (β_c), and inhibition efficiency (EI) found in Table 3.

$$EI\% = \frac{I_{corr,0} - I_{corr}}{I_{corr,0}} \times 100 \quad (9)$$

$I_{corr,0}$ and I_{corr} show the corrosion current density with and without inhibitor.

The corrosion current density on the Tafel curve decreases with increasing BCS concentration, indicating that BCS is adsorbed to form a protective layer on the copper surface. The shift in the polarization potential of the anodic curve with increasing BCS concentration indicates the desorption of the inhibitor on the copper surface (Tan et al., 2020). The shift in corrosion potential (E_{corr}) towards the negative is related to the ability of the inhibitor to reduce oxygen on the cathodic side of the metal. The shift in corrosion potential of copper with and without the addition of BCS has a difference of less than 85 mV, which indicates that BCS is a mixed corrosion inhibitor for copper in 1 M H₂ SO₄.

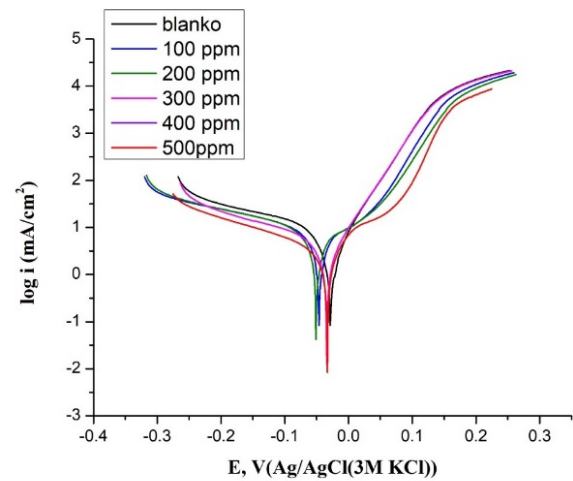
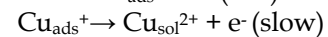
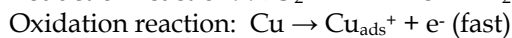
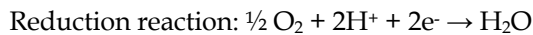


Figure 2. Tafel Curves in 1M H₂ SO₄ Solution with and without BSC at Different Concentrations.

The corrosion mechanism of copper in acid occurs through the formation of insoluble Cu⁺ ions on the copper surface on the anodic side. Further oxidation reaction of Cu⁺ ions occurs to form Cu²⁺ ions that diffuse and dissolve in solution. Dissolved oxygen in the solution diffuses to the copper surface, resulting in a reduction reaction on the cathodic side ((Tan et al., 2018); Zioud et al., 2020).



Isothermal Adsorption

The adsorption type of BCS on the copper surface can be determined from the resulting adsorption isothermal model. The recovery of the metal surface is calculated from the difference in inhibitor concentration

using the relationship $\theta = EI\%/100$ ($EI\%$ obtained from the polarization curve). Adsorption isothermal models that are often used are Langmuir, Temkin, Frumkin, Freundlich, El-Adawi, and Flory-Huggin. The adsorption of BCS on the copper surface adapts the Langmuir adsorption isothermal model characterized by a correlation coefficient equal to 0.982. The Langmuir adsorption isotherm was determined from equation (10).

$$\frac{C}{\theta} = \frac{1}{K_{ads}} + C \tag{10}$$

Where C is the inhibitor concentration, θ is coverage degree, and K_{ads} is the adsorption equilibrium constant adsorption of inhibitors on metal surfaces based on Langmuir theory occurs on the specific homogeneous side of the metal with the same adsorption energy. The inhibitor forms a monolayer on the metal surface. This type of adsorption indicates no interaction energy between molecules, and only adsorption and desorption reactions of inhibitors occur on the metal surface (Li et al., 2020). The K_{ads} value obtained is $10,93 \times 10^3 \text{ L.mol}^{-1}$. The slope of the Langmuir plot is 1,2996, indicating that only one BCS molecule replaces exactly one water molecule on the copper surface (Toghan et al., 2024).

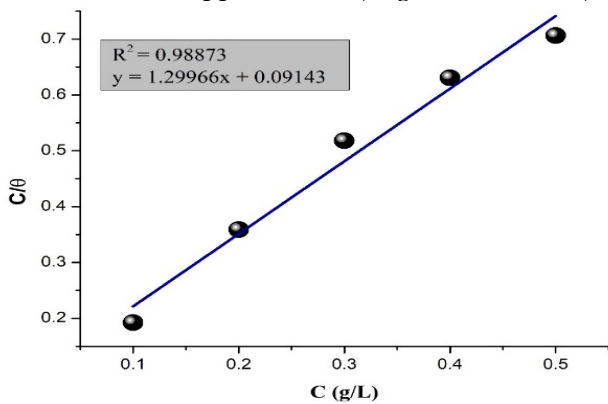


Figure 3. Langmuir Model Adsorption Isothermal Plot of Copper in 1M H₂SO₄ Solution with Addition of Different BCS Concentration at 298K

Table 3. Electrochemical Parameters of Copper in 1 M H₂SO₄ with Addition of Different BCS Concentration at 298K

C (ppm)	E _{corr} (mV(Ag/AgCl))	I _{cor} (μA/c m ²)	-β _a (mV/dec)	β _c (mV/dec)	EI (%)
Blank	20.9	9.82	350	600	-
100	-46	4.70	139	141	52
200	-51	4.35	120	138	55.70
300	-60	4.13	189	141	57.94
400	-37	3.59	200	89.1	63.44
500	-33	2.86	194	88	70.87

Free energy of adsorption (ΔG_{ads}), enthalpy adsorption (ΔH_{ads}), and entropy adsorption (ΔS_{ads}) can

be calculated using the correlation to K_{ads} in equation (11) where R and T are the universal gas constant ($8.314 \text{ J mol}^{-1} \text{ K}^{-1}$) and thermodynamic temperature (K)(Gapsari et al., 2024; Toghan et al., 2024; Sait et al., 2022).

$$\Delta G_{ads} = -RT \ln (55.5K_{ads}) \tag{11}$$

$$\Delta H_{ads} = -(\ln K_{ads}) RT \tag{12}$$

$$\Delta S_{ads} = \frac{\Delta H_{ads} - \Delta G_{ads}}{T} \tag{13}$$

Based on the calculation results, the value of ΔG_{ads} is -15.87 kJ/mol , which is less than -20 kJ/mol , indicates that BCS adsorption belongs to physical adsorption (electrostatic attraction) (Gapsari et al., 2024). The negative sign in the value ΔG_{ads} indicates that the adsorption of the BCS copper surface occurs spontaneously. The enthalpy of adsorption ΔH_{ads} and entropy of adsorption ΔS_{ads} are -5.92 kJ/mol and 0.33 kJ/mol , respectively. The adsorption process takes place exothermically based on the negative sign of enthalpy value and forming a protective layer on copper.

Quantum chemical parameters

Quantum chemical parameters can be used to predict the adsorption mechanism of inhibitors based on their molecular structure. The investigation of quantum chemical parameters in this study was carried out on linoleic acid, methyl linoleate, palmitic acid, methyl palmitic, and 4-cyclopentene-1,3-dione molecules on a copper surface. The optimized molecular geometry structure, the electron density of the highest occupied molecular orbital (HOMO), lowest unoccupied molecular orbital (LUMO), dan electrostatic potential (ESP) obtained from Density Functional Theory (DFT) results are shown in Tabel 4.

The molecular structure's nucleophilic (negative side) and electrophilic (positive side) in the ESP image are marked in red and blue. The red colour region is electron-rich, while the blue colour region has a low electron density. The order of electron density in molecular electrostatic potential is red > orange > yellow > green > blue. In general, metals are electrophilic agents with empty d orbitals, making them accessible to attract negatively charged sites of inhibitor molecules. The molecular structure of inhibitors that have heteroatom groups, conjugate double bonds will form coordination covalent bonds with metals (Zhang & Li, 2020).

The HOMO center of linoleic acid (AOCT) dan methyl linoleate (MLIN) is π depicted in Figure 4. The MLIN molecules have the highest high-occupied molecular orbital energy (E_{HOMO}) among all the inhibitor molecules studied. It is generally known that the ability of inhibitor molecules to transfer electrons to the copper surface can be obtained from E_{HOMO} . The inhibitor

molecules make it easier to transfer electrons if E_{HOMO} is high. Low Unoccupied Molecular Orbital energy (E_{LUMO}) indicate the ability of a molecule to accept electrons. The inhibitor molecules will be easier to accept electrons from the metal (back donation) if E_{LUMO} is low (Tuzun & Bhawsar, 2021). The 4-cyclopentene-1,3-dione (CPTD) has the lowest E_{LUMO} , making it easier to accept electrons.

The low HOMO and LUMO orbital energy difference (ΔE) of the molecules indicates that the molecules are more polarizable and reactive, so the adsorption layer formed is more stable. The CPTD molecules have an energy gap of 4,079 eV. The low ionization potential (I) value and high electron affinity (A) indicate the molecule's ability to donate and accept electrons (Diki et al., 2021). The electron donor effect of the inhibitor can be analyzed from the electron transfers value. If $\Delta N < 3.6$, the inhibition ability can increase the electron donor ability on the metal surface. Electron donor groups such as $-CH_3$ and $-OH$ can improve the corrosion inhibition efficiency and increase the amount

of electron transfer to the metal surface (Hadisaputra, et al, 2019). Electronegativity is also an important parameter that indicates the ability of a molecule to attract electrons. The lowest electronegativity value of the inhibitor molecule studied in the MLIN molecule (2.903 eV) will more easily form a bond with copper with a higher electronegativity (4,98 eV).

Table 4. Quantum Chemical Parameters of Inhibitors Determined by DFT/B3LYP/6-31G(d) Method

Parameter	Inhibitors				
	AOCT	APLM	CPTD	MPLM	MLIN
E_{HOMO} (eV)	-6.296	-7.438	-6.503	-7.288	-6.244
E_{LUMO} (eV)	0.334	0.342	-2.424	0.398	0.437
ΔE (eV)	6.631	7.780	4.079	7.686	6.682
I (eV)	6.296	7.438	6.503	7.288	6.244
A (eV)	-0.334	-0.342	2.424	-0.398	-0.437
μ (Debye)	1.386	1.365	2.432	1.519	1.925
χ (eV)	2.981	3.547	4.464	3.445	2.903
η (eV)	3.315	3.890	2.039	3.843	3.341
σ (eV ⁻¹)	0.302	0.257	0.490	0.260	0.299
ΔN (e)	0.301	0.184	0.126	0.199	0.310

Table 5. Adsorption energy of copper corrosion system simulated by molecular dynamics of inhibitor and H₂O

Inh	Adsorption Energy (Kcal/mol)	Deformation Energy (Kcal/mol)	Inh: dE_{ad}/dN_i (Kcal mol ⁻¹)	H ₂ O: dE_{ad}/dN_i (Kcal/mol)
MLIN	-3709.400	-2714.736	-116.1463	-29.9766
AOCT	-3720.283	-2719.307	-114.6973	-29.5283
MPLM	-3723.363	-2718.456	-108.8362	-31.0922
CPTD	-3668.160	-2719.169	-64.5912	-30.8206
APLM	-3721.456	-2716.073	-103.0507	-31.7377

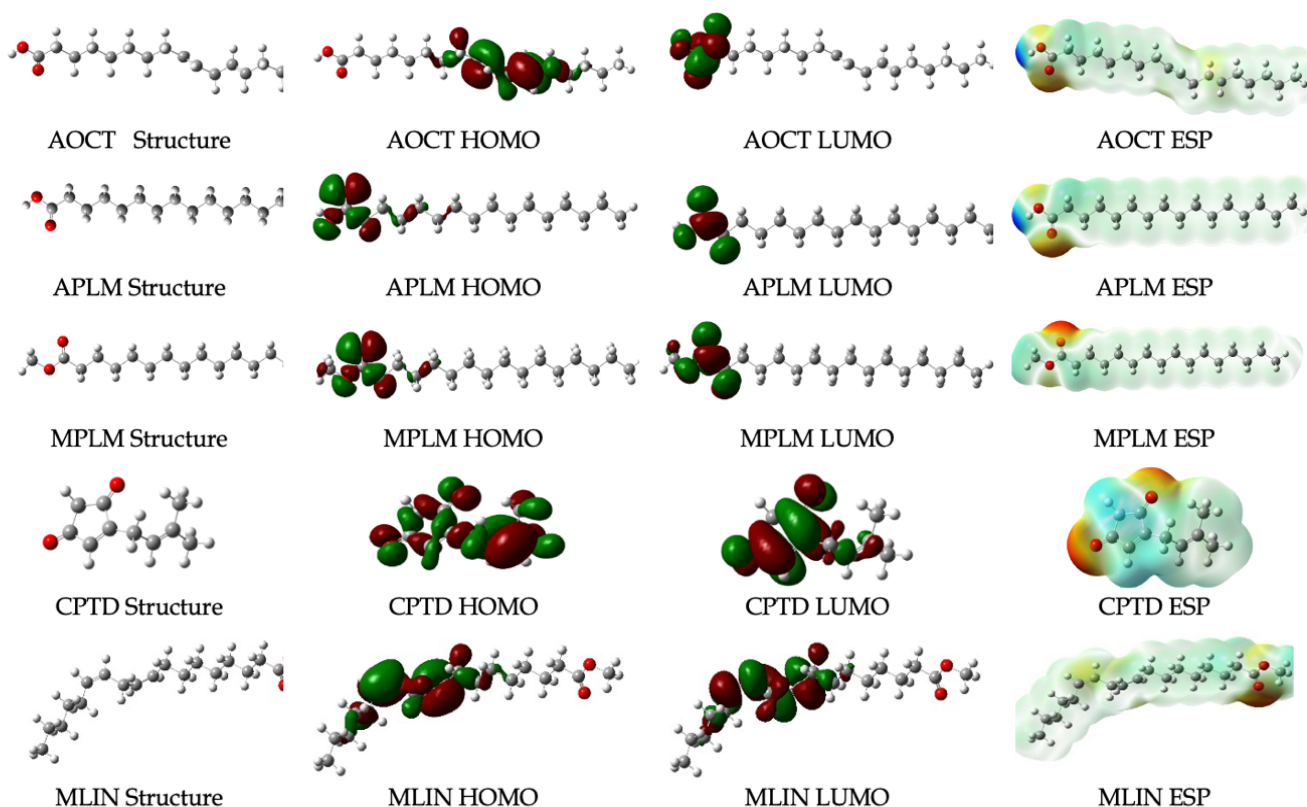


Figure 4. Optimized Structure, HOMO, LUMO and ESP

Monte Carlo Simulation

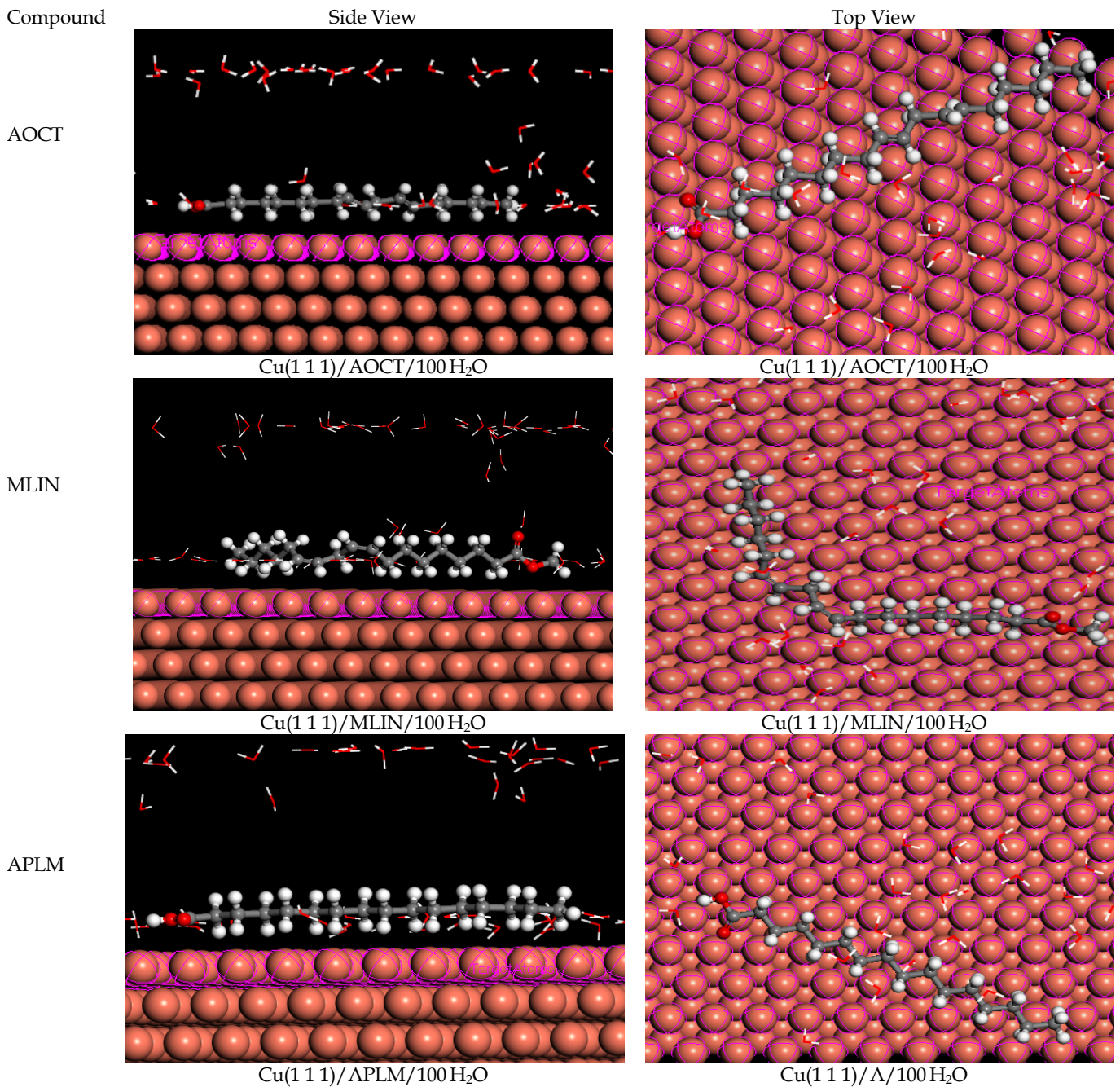
Molecular dynamic simulation is used to understand the dynamic movement of atoms or molecules with computational calculation within a certain period. The molecular dynamics simulation process in a corrosion system consists of water molecules, corrosive ions and inhibitor molecules moving until they reach equilibrium in a stable state. Binding energy (E_{bind}) is required to desorb inhibitor molecules from the metal surface due to the bond formed. This energy is reciprocal to the adsorption energy (E_{ads}). An increasingly positive (high) binding energy value causes the interaction force between the

inhibitor molecule and the metal surface to be stronger. In contrast, the adsorption energy of the inhibitor will be lower (stable) (Haris et al., 2021).

$$E_{ads} = E_{tot} - (E_{sub} + E_{inh}) \tag{14}$$

$$E_{bind} = -E_{ads} \tag{15}$$

Where E_{tot} dan E_{sub} indicates the system's total energy and the metal substrate's energy, negative adsorption energy values indicate that the inhibitor molecules are thermodynamically spontaneously adsorbed.



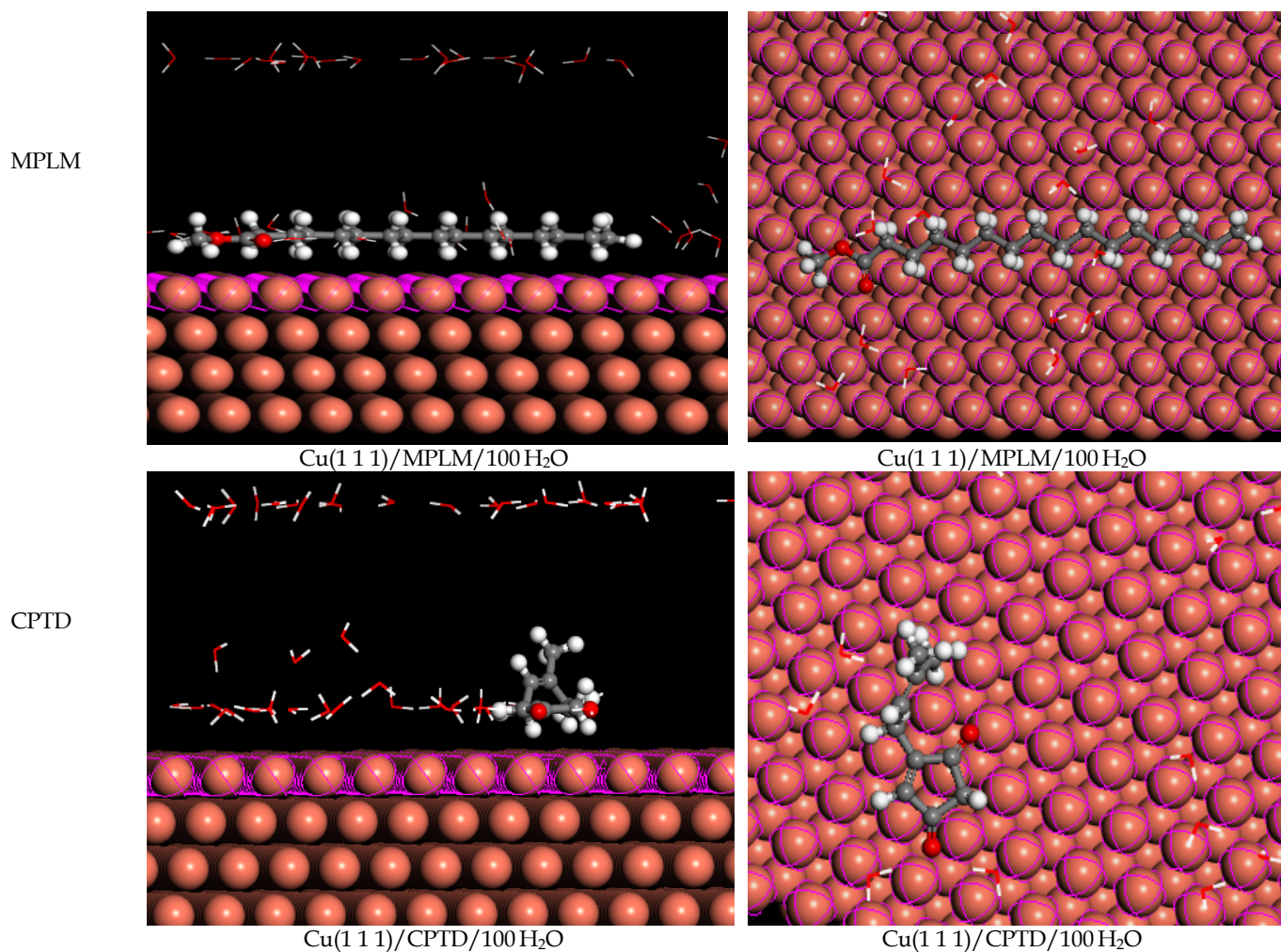


Figure 5. Adsorption Visualization of Inhibitor Molecules from Side and Top View

The total adsorption energy, adsorption energy of inhibitor molecules, and adsorption energy of water molecules on the Cu (111) surface are present in Table 5. MLIN molecules have stable adsorption energy (lowest) among the inhibitor molecules studied. It is consistent with the highest E_{HOMO} of MLIN molecule, so it is more easily adsorbed. The orientation of MLIN molecule on the Cu (111) is horizontal on the alkene and ester group. The other inhibitor molecules, such as palmitic acid (APLM), linoleic acid (AOCT), and methyl palmitate (MPLM), are adsorbed in parallel on the copper surface (Figure 5). The parallel (horizontal) adsorption of inhibitor molecules on the metal surface results in better corrosion inhibition because the metal surface area covered by the inhibitor molecules is large, and the binding energy generated is also higher (Verma et al., 2018).

Conclusion

Experimental and theoretical studies have been conducted to investigate BCS's inhibition ability and

inhibition mechanism against copper corrosion in 1 M H_2SO_4 . The following conclusions were obtained.

- (1). Electrochemical measurements showed that BCS is a mixed inhibitor (cathodic and anodic), producing an inhibition efficiency that increases with increasing BCS due to the formation of a protective layer. The highest inhibition efficiency at 500 ppm BCS was 73,3%.
- (2). The isothermal adsorption of BCS molecules is physisorption that occurs spontaneously and corresponds to Langmuir isothermal adsorption.

The theoretical calculation shows that the MLIN molecule has strong adsorption on the copper surface because it has alkene and ester groups. Other molecules also show strong adsorption characterized by parallel adsorption, resulting in high inhibition efficiency.

References

- Al-Amiery, A. A., Al-Azzawi, W. K., & Isahak, W. N. R. W. (2022). Isatin Schiff base is an effective corrosion inhibitor for mild steel in hydrochloric acid solution: gravimetric, electrochemical, and

- computational investigation. *Scientific Reports*, 12(1). <https://doi.org/10.1038/s41598-022-22611-4>
- Alrashidi, M., Derawi, D., Salimon, J., & Yusoff, M. F. (2022). The effects of different extraction solvents on the yield and antioxidant properties of *Nigella sativa* oil from Saudi Arabia. *Journal of Taibah University for Science*, 16(1), 330–336. <https://doi.org/10.1080/16583655.2022.2057673>
- Bilgic, S. (2018). *The Methods for Prevention of Corrosion. Technology, Engineering & Mathematics (EPSTEM)*, 4. Retrieved from www.isres.org
- BustosRivera-Bahena, G., Ramirez-Arteaga, A. M., Saldarriaga-Noreña, H. A., Larios-Gálvez, A. K., González-Rodríguez, J. G., Romero-Aguilar, M., & Sesenes, R. L. (2024). Hexane extract of *Persea schiedeana* Ness as green corrosion inhibitor for the brass immersed in 0.5 M HCl. *Scientific Reports*, 14(1). <https://doi.org/10.1038/s41598-024-56793-w>
- Diki, N. Y. S., Coulibaly, N. H., Kambiré, O., & Trokourey, A. (2021). Experimental and Theoretical Investigations on Copper Corrosion Inhibition by Cefixime Drug in 1M HNO₃ Solution. *Journal of Materials Science and Chemical Engineering*, 09(05), 11–28. <https://doi.org/10.4236/msce.2021.95002>
- Emad, M., & AL-Rasheedi, M. (2015). *Nigella Sativa* and Natural Honey as Corrosion Inhibitors for Copper in Cooling Water Systems. *J. Mater. Environ. Sci*, 6(1), 201–206.
- Fu, D., Tan, B., Lu, L., Qin, X., Chen, S., He, W., & Chen, J. (2018). Study on the corrosion inhibition effect of 2,3-Dimercapto-1- propanol on copper in 0.5mol/L H₂SO₄ solution. *International Journal of Electrochemical Science*, 13(9), 8561–8574. <https://doi.org/10.20964/2018.09.16>
- Gapsari, F., Setyarini, P. H., Utaminigrum, F., Sulaiman, A. M., Haidar, M. F., & Julian, T. S. (2024). Melaleuca leaves extract as eco-friendly inhibitor for low carbon steel in sulfuric acid. *Case Studies in Chemical and Environmental Engineering*, 9. <https://doi.org/10.1016/j.cscee.2024.100657>
- Hadisaputra, S., Iskandar, Z., & Asnawati, D. (2019). Prediction of the corrosion inhibition efficiency of imidazole derivatives: A Quantum Chemical Study. *Acta Chimica Asiana*, 2(1), 88–94.
- Hadisaputra, S., Purwoko, A. A., Hakim, A., Prasetyo, N., & Hamdiani, S. (2022). Corrosion Inhibition Properties of Phenyl Phthalimide Derivatives against Carbon Steel in the Acidic Medium: DFT, MP2, and Monte Carlo Simulation Studies. *ACS Omega*, 7(37), 33054–33066. <https://doi.org/10.1021/acsomega.2c03091>
- Haris, N. I. N., Sobri, S., Yusof, Y. A., & Kassim, N. K. (2021). An overview of molecular dynamic simulation for corrosion inhibition of ferrous metals. In *Metals* (Vol. 11, Issue 1, pp. 1–22). MDPI AG. <https://doi.org/10.3390/met11010046>
- Kabir, Y., Akasaka-Hashimoto, Y., Kubota, K., & Komai, M. (2020). Volatile compounds of black cumin (*Nigella sativa* L.) seeds cultivated in Bangladesh and India. *Heliyon*, 6(10). <https://doi.org/10.1016/j.heliyon.2020.e05343>
- Li, H., Zhang, S., Tan, B., Qiang, Y., Li, W., Chen, S., & Guo, L. (2020). Investigation of Losartan Potassium as an eco-friendly corrosion inhibitor for copper in 0.5 M H₂SO₄. *Journal of Molecular Liquids*, 305. <https://doi.org/10.1016/j.molliq.2020.112789>
- Mazaheri, Y., Torbati, M., Azadmard-Damirchi, S., & Savage, G. P. (2019). A comprehensive review of the physicochemical, quality and nutritional properties of *Nigella sativa* oil. In *Food Reviews International* (Vol. 35, Issue 4, pp. 342–362). Taylor and Francis Inc. <https://doi.org/10.1080/87559129.2018.1563793>
- Mollaamin, F. (2023). Increasing corrosion resistance of binary Al-Alloy through implanting with some transition elements and heteroatom organic compounds. *Acta Chimica Asiana*, 6(2), 328–342.
- Mzioud, K., Habsaoui, A., Ouakki, M., Galai, M., El Fartah, S., & Ebn Touhami, M. (2020). Inhibition of copper corrosion by the essential oil of *Allium sativum* in 0.5M H₂SO₄ solutions. *SN Applied Sciences*, 2(9). <https://doi.org/10.1007/s42452-020-03393-8>
- Nivetha, K., & Prasanna, G. (2016). International Journal of Advanced Research in Biological Sciences GC-MS and FT-IR Analysis of *Nigella sativa* L. Seeds. *Int. J. Adv. Res. Biol. Sci*, 3(6), 45–54. <http://s-o-i.org/1.15/ijarbs-2016-3-6-7>
- Orozco-Cruz, R., Ávila, E., Mejía, E., Pérez, T., Contreras, A., & Galván-Martínez, R. (2017). In situ corrosion study of copper and copper-alloys exposed to natural seawater of the Veracruz port (Gulf of Mexico). *International Journal of Electrochemical Science*, 12(4), 3133–3152. <https://doi.org/10.20964/2017.04.27>
- Radi, M., Melian, R., Galai, M., Dkhirche, N., Makha, M., Verma, C., Fernandez, C., & EbnTouhami, M. (2021). Pumpkin seeds as an eco-friendly corrosion inhibitor for 7075-T6 alloy in 3.5% NaCl solution: Electrochemical, surface and computational studies. *Journal of Molecular Liquids*, 337. <https://doi.org/10.1016/j.molliq.2021.116547>
- Rehioui, M., About, S., Benzidia, B., Hammouch, H., Erramli, H., Daoud, N. A., Badrane, N., & Hajjaji, N. (2021). Corrosion inhibiting effect of a green formulation based on *Opuntia Dillenii* seed oil for iron in acid rain solution. *Heliyon*, 7(4). <https://doi.org/10.1016/j.heliyon.2021.e06674>
- Sait, N., Aliouane, N., Ait Ahmed, N., & Al-Noaimi, M. (2022). Electrochemical investigation of di-

- phosphonic acid on corrosion inhibition behavior of copper in hydrochloric acid medium. *Journal of the Iranian Chemical Society*, 19(2), 463–473. <https://doi.org/10.1007/s13738-021-02322-9>
- Saleh, F. A., El-Darra, N., Raafat, K., & El Ghazzawi, I. (2018). Phytochemical analysis of *Nigella sativa* L. Utilizing GC-MS exploring its antimicrobial effects against multidrug-resistant bacteria. *Pharmacognosy Journal*, 10(1), 99–105. <https://doi.org/10.5530/pj.2018.1.18>
- Sedik, A., Athmani, S., Saoudi, A., Ferkous, H., Ribouh, N., Lerari, D., Bachari, K., Djellali, S., Berredjem, M., Solmaz, R., Alam, M., Jeon, B. H., & Benguerba, Y. (2022). Experimental and theoretical insights into copper corrosion inhibition by protonated amino-acids. *RSC Advances*, 12(36), 23718–23735. <https://doi.org/10.1039/d2ra03535a>
- Souli, R., Leila, D., Berçot, P., Rezrazi, M., & Triki, E. (2017). Effect of aqueous extract of *Nigella sativa* seeds on the mild steel corrosion in chloride media. *In Journal of the Tunisian Chemical Society* (Vol. 19).
- Swathi, P. N., Rasheeda, K., Samshuddin, S., & Alva, V. D. P. (2017). Fatty Acids and its Derivatives as Corrosion Inhibitors for Mild Steel - An Overview. *Journal of Asian Scientific Research*, 7(8), 301–308. <https://doi.org/10.18488/journal.2.2017.78.301.308>
- Tan, B., Zhang, S., Qiang, Y., Guo, L., Feng, L., Liao, C., Xu, Y., & Chen, S. (2018). A combined experimental and theoretical study of the inhibition effect of three disulfide-based flavouring agents for copper corrosion in 0.5 M sulfuric acid. *Journal of Colloid and Interface Science*, 526, 268–280. <https://doi.org/10.1016/j.jcis.2018.04.092>
- Tan, B., Zhang, S., Qiang, Y., Li, W., Li, H., Feng, L., Guo, L., Xu, C., Chen, S., & Zhang, G. (2020). Experimental and theoretical studies on the inhibition properties of three diphenyl disulfide derivatives on copper corrosion in acid medium. *Journal of Molecular Liquids*, 298. <https://doi.org/10.1016/j.molliq.2019.111975>
- Toghan, A., Alhussain, H., Attia, A., Alduaij, O. K., Fawzy, A., Eldesoky, A. M., & Farag, A. A. (2024). Corrosion inhibition performance of copper using N-benzylhydrazinecarbothioamide in a 3.5 % NaCl solution. *Journal of Electrochemical Science and Engineering*, 14(2), 231–245. <https://doi.org/10.5599/jese.2181>
- Tüzün, B., & Bhawsar, J. (2021). Quantum chemical study of thiazole derivatives as corrosion inhibitors based on density functional theory. *Arabian Journal of Chemistry*, 14(2). <https://doi.org/10.1016/j.arabjc.2020.102927>
- Vaghefinazari, B., Wierzbicka, E., Visser, P., Posner, R., Arrabal, R., Matykina, E., Mohedano, M., Blawert, C., Zheludkevich, M. L., & Lamaka, S. V. (2022). Chromate-Free Corrosion Protection Strategies for Magnesium Alloys – A Review: Part III – Corrosion Inhibitors and Combining Them with Other Protection Strategies. *In Materials* (Vol. 15, Issue 23). MDPI. <https://doi.org/10.3390/ma15238489>
- Vargas, I. T., Fischer, D. A., Alsina, M. A., Pavissich, J. P., Pablo, P., & Pizarro, G. E. (2017). Copper corrosion and biocorrosion events in premise plumbing. *In Materials* (Vol. 10, Issue 9). MDPI AG. <https://doi.org/10.3390/ma10091036>
- Verma, C., Lgaz, H., Verma, D. K., Ebenso, E. E., Bahadur, I., & Quraishi, M. A. (2018). Molecular dynamics and Monte Carlo simulations as powerful tools for study of interfacial adsorption behavior of corrosion inhibitors in aqueous phase: A review. *In Journal of Molecular Liquids* (Vol. 260, pp. 99–120). Elsevier B.V. <https://doi.org/10.1016/j.molliq.2018.03.045>
- Xu, P., Fu, Q., & Zhao, M. (2023). The influence of calcium on copper corrosion and its by-product release in drinking water. *RSC Advances*, 13(26), 17842–17855. <https://doi.org/10.1039/d3ra01696j>
- Zhang, J., & Li, H. (2020). 2-(2-chlorophenyl)-1H-benzimidazole as a new corrosion inhibitor for copper in sulfuric acid. *International Journal of Electrochemical Science*, 15, 5362–5372. <https://doi.org/10.20964/2020.06.63>
- Zomorodian, A., & Behnood, A. (2023). Review of Corrosion Inhibitors in Reinforced Concrete: Conventional and Green Materials. *In Buildings* (Vol. 13, Issue 5). MDPI. <https://doi.org/10.3390/buildings13051170>